

Dynamic mechanical response of polystyrene at high strain rates under uniaxial strain ramp loading

Xuping Zhang(张旭平), Fuli Tan(谭福利), Binqiang Luo(罗斌强), Guiji Wang(王桂吉), Jianheng Zhao(赵剑衡), and Chengwei Sun(孙承纬)

Citation: Chin. Phys. B, 2026, 35 (**4**): 046201. DOI: 10.1088/1674-1056/ae0637
http://cpb.iphy.ac.cn; http://iopscience.iop.org/cpb

What follows is a list of articles you may be interested in

Structural stability and properties of Li_2XN_6 (X = Be, Mg, Ca) ternary nitrides

Rui Wang(王睿), Cai-Zi Zhang(张才姿), Qi-Wen Jiang(蒋其雯), En-Yu Wang(王恩宇), Jie Wei(魏杰), and Hong-Yang Zhu(祝洪洋)

Chin. Phys. B, 2026, 35 (**3**): 036201. DOI: 10.1088/1674-1056/ae1f03

Molecular dynamics study of coupled layer thickness and strain rate effect on tensile behaviors of Ti/Ni multilayered nanowires

Meng-Jia Su(宿梦嘉), Qiong Deng(邓琼), Lan-Ting Liu(刘兰亭), Lian-Yang Chen(陈连阳), Meng-Long Su(宿梦龙), and Min-Rong An(安敏荣)

Chin. Phys. B, 2021, 30 (**9**): 096201. DOI: 10.1088/1674-1056/abf10a

Unusual softening behavior of yield strength in niobium at high pressures

Qiu-Min Jing(敬秋民), Qiang He(何强), Yi Zhang(张毅), Shou-Rui Li(李守瑞), Lei Liu(柳雷), Qi-Yue Hou(侯琪玥), Hua-Yun Geng(耿华运), Yan Bi(毕延), Yu-Ying Yu(俞宇颖), Qiang Wu(吴强)

Chin. Phys. B, 2018, 27 (**10**): 106201. DOI: 10.1088/1674-1056/27/10/106201

Strain-rate-induced bcc-to-hcp phase transformation of Fe nanowires

Hongxian Xie(谢红献), Tao Yu(于涛), Wei Fang(方伟), Fuxing Yin(殷福星), Dil Faraz Khan

Chin. Phys. B, 2016, 25 (**12**): 126201. DOI: 10.1088/1674-1056/25/12/126201

Effects of tilt interface boundary on mechanical properties of Cu/Ni nanoscale metallic multilayer composites

Yang Meng (杨萌), Xu Jian-Gang (徐建刚), Song Hai-Yang (宋海洋), Zhang Yun-Guang (张云光)

Chin. Phys. B, 2015, 24 (**9**): 096202. DOI: 10.1088/1674-1056/24/9/096202

Dynamic mechanical response of polystyrene at high strain rates under uniaxial strain ramp loading

Xuping Zhang(张旭平)[1,†], Fuli Tan(谭福利)[1], Binqiang Luo(罗斌强)[1], Guiji Wang(王桂吉)[1], Jianheng Zhao(赵剑衡)[2], and Chengwei Sun(孙承纬)[1]

[1] *Institute of Fluid Physics, China Academy of Engineering Physics, Mianyang* 621999, *China*
[2] *Institute of Applied Electronics, China Academy of Engineering Physics, Mianyang* 621999, *China*

(Received 12 June 2025; revised manuscript received 25 August 2025; accepted manuscript online 12 September 2025)

Determination of the yield strength of polymers under dynamic loading has proven to be extremely difficult. Until now, few strength data have been obtained for polymers at strain rates above 10^5 s^{-1}. Based on the electromagnetically driven quasi-isentropic loading technique, the yield strength of polystyrene under high pressure and high strain rate is measured experimentally using a pressure comparison method. In the experiment, a polystyrene window method is used to measure the *in-situ* particle velocity directly, which reduces the experimental error and obtains reliable high-pressure Lagrangian sound velocity and a quasi-isentropic compression line. The yield stress of polystyrene under quasi-isentropic compression is measured continuously at pressure up to 4 GPa and a strain rate of 10^6 s^{-1}. Combined with strength data under quasi-static and intermediate strain rate loading, the strain rate effect of the yield of polystyrene is analyzed. It is found that the yield strength of polystyrene shows strain rate effects, but the "up-turn" phenomenon is not observed. Additionally, the yield stress of polystyrene from 10^{-3} s^{-1} to 10^6 s^{-1} strain rate can be fitted using the Eyring model, which provides a reference for the study of the physical properties of polymer materials under high strain rate loading.

Keywords: yield strength, quasi-isentropic compression, Lagrangian sound speed, high strain rate

PACS: 62.50.–p, 51.30.+i,62.20.–x

DOI: 10.1088/1674-1056/ae0637 **CSTR:** 32038.14.CPB.ae0637

1. Introduction

The yield strength of polystyrene under high-pressure and high strain rate conditions is of great interest to technological applications and basic science due to its potential applications: for instance, hypervelocity impact problems of transparent lightweight armor design,[1] performance prediction of some composites[2] and hydrodynamic instability properties of ablator material for laser-based high energy density physics experiments.[3,4]

Some of the earliest papers on dynamic loading studied the material response of polymers, including Kolsky's paper in 1949[5] and the work by Davies and Hunter in 1963.[6] Over the past 70 years, the mechanical response (principally the relationship between stress and strain) of a number of polymers has been characterized at strain rates between 10^{-4} s^{-1} and 10^5 s^{-1}.[7–10] Walley investigated polystyrene (PS) in the low and intermediate strain rate regime from 10^{-2} s^{-1} to 10^4 s^{-1}.[8,10] He concluded that polymers show higher yield stress at high strain rates than at low strain rates under static loading. In 2004, Bourne and Millett conducted studies on the flow stress behavior of polystyrene under shock compression. They obtained the shear strength of polystyrene at different longitudinal stresses up to 4 GPa.[11,12] In 2018, Zhang obtained the yield strength of polystyrene at a strain rate of 10^6 s^{-1} under quasi-isentropic compression from elastic–plastic transition characteristics on the stress wave profiles.[13] However, the determination of mechanical properties, such as yield strength at high pressure under dynamic loading, has proven to be extremely difficult. High-pressure yield strength data have been obtained for a few metals and ceramics under shock loading and in limited stress ranges.[14,15] Characterization of polymers at high pressure and high strain rates presents a number of challenges associated with their relatively low sound speed and low intrinsic strength, leading to poor signal-to-noise ratios. Due to some limitations of the loading and diagnostic methods, in particular, modulus data, such as sound velocity, have not been obtained.[16,17]

More recently, magnetic[18] and laser[19] compression techniques have been used to determine material strength properties under isentropic loading. They can produce high pressures from several GPa to TPa and high strain rates from 10^4 s^{-1} to 10^7 s^{-1}. Using the magnetic loading technique, an extensive investigation on the strength of aluminum under isentropic compression was recently conducted by Asay *et al.*[20] In contrast to shock compression, magnetically driven quasi-isentropic compression is extremely sensitive to detecting an elastic–plastic transition or phase change of materials due to its loading waves with long rise times, wherein very small and abrupt volume changes lead to large signatures in velocity profiles.[21–23] Thus, subtle details in the dynamic responses of samples can be revealed in quasi-isentropic com-

†Corresponding author. E-mail: xupingzhang@sina.cn

© 2026 Chinese Physical Society and IOP Publishing Ltd. All rights, including for text and data mining, AI training, and similar technologies, are reserved.

pression experiments. One way to determine material strength under quasi-isentropic loading is to subtract the hydrostatic pressure from longitudinal stress. This method requires high-precision parameters of equation-of-state or high-precision static compression experimental data to calculate hydrostatic pressure. On the other hand, one must ensure that the experimentally determined longitudinal stress response is accurate as well. However, for polymers, the measurement of strength and sound velocity needs to obtain the *in-situ* particle velocity for material modulus calculation.[24–26] Taking polystyrene as an example, both velocity measurement and *in-situ* particle velocity acquisition are challenging.

The objective of this work is to obtain and better understand the high-pressure sound speed, and isentropic and yield behavior of polystyrene under quasi-isentropic compression. This understanding is crucial for designing and simulating various applications of polystyrene and its composites. A description of experimental techniques and conditions of magnetically driven quasi-isentropic compression experiments is presented in Section 2. Section 3 presents a discussion of isentropic compression experimental results, including high-pressure sound speed, quasi-isentropic compression, yield stress and its strain rate effects. The main insights and conclusions are summarized in Section 4.

2. Experimental techniques and conditions

2.1. Experimental approach

Under uniaxial strain compression, the material yield strength can be expressed as[24]

$$Y = \frac{3}{2}(\sigma_{xx} - P), \tag{1}$$

where σ_{xx} is the longitudinal stress, and P is the hydrostatic pressure.

Under magnetically driven quasi-isentropic compression, the longitudinal stress along the loading path can be measured, and then the yield strength can be calculated as[25,26]

$$Y = \frac{3}{2}(\sigma_{xx} - P_{\rm s} - \Delta P_{\rm th}), \tag{2}$$

where $P_{\rm s}$ is the theoretical isentrope, and $\Delta P_{\rm th}$ is the pressure increment caused by heat dissipation.

A schematic of magnetically driven isentropic compression experiments is shown in Fig. 1. A pulse current with mega-ampere amplitude flows on the inner surface of the anode and cathode, and then a pulsed magnetic field is produced in the space between the anode and cathode. The interaction between the current and magnetic field produces huge Lorentz force, which acts on the inner surfaces of the electrodes and can be equivalent to magnetic pressure. There are two sample arrangements in the experiment, with or without a transparent window. Pressure waves transmit from the electrode to the sample, and the rear surface velocity of the samples are measured using a photon Doppler velocimeter (PDV). When the measured velocity profiles are converted to *in situ* particle velocity, the Lagrangian sound speed can be calculated as

$$C_{\rm L}(u) = \Delta h/\Delta t(u), \tag{3}$$

where $C_{\rm L}$ is the Lagrangian sound speed, u is the *in-situ* particle velocity, Δh is the initial thickness difference of different samples, and Δt is the difference in time at the same *in-situ* particle velocity for different samples. Knowing the initial ambient density of the material, the stress–strain response is determined from the conservation equations through the Riemann relations[20,27,28]

$$\sigma = \int_0^u \rho_0 C_{\rm L}(u)\,{\rm d}u, \tag{4}$$

$$\varepsilon = \int_0^u C_{\rm L}^{-1}(u)\,{\rm d}u, \tag{5}$$

where σ is the longitudinal stress, ρ_0 is the initial density, and ε is the strain.

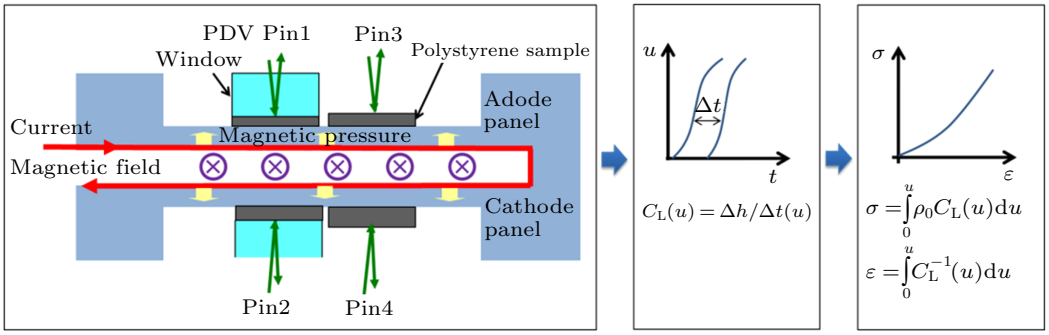


Fig. 1. A schematic diagram of magnetically driven quasi-isentropic compression experiments.

2.2. Materials

The basic material property data of the polystyrene samples are presented in Table 1. The acoustic properties were measured by a pulse receiver with quartz transducers at a frequency of 5 MHz. The mechanical properties of polystyrene under a quasi-static state and medium strain rate were obtained using a material testing machine and split Hopkinson pressure

bar (SHPB), respectively. In the quasi-static experiments, the sample size is $\phi 10 \times 30$ mm and the measured stress–strain curve is shown in Fig. 2. In the Hopkinson bar experiments, the compression bar was an aluminum bar with a diameter of 14.5 mm, and the sample size was $\phi 7 \times 10$ mm. The stress–strain curve of polystyrene with a strain rate of 2000 s^{-1} is also shown in Fig. 2. As seen in Fig. 2, the maximum flow stress under quasi-static and dynamic loading is 0.106 GPa at a strain rate of 10^{-3} s^{-1} and 0.133 GPa at a strain rate of 2×10^3 s^{-1}, respectively.

Table 1. Characteristics of as-received polystyrene. Here, C_{L0} denotes longitudinal sound speed, C_s denotes shear sound speed, C_b denotes bulk sound speed and ν denotes Poisson's ratio.

Density (g/cm^3)	C_{L0} (km s^{-1})	C_s (km s^{-1})	C_b (km s^{-1})	ν
1.05	2.322	1.136	1.917	0.343

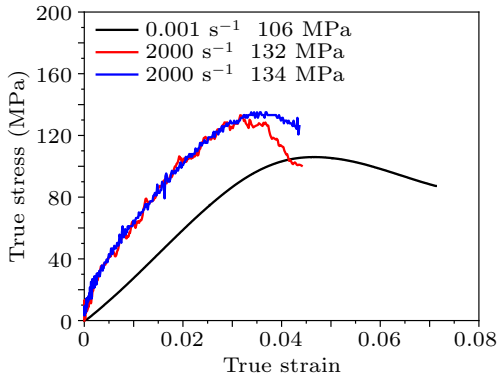


Fig. 2. Stress–strain curves (quasi-static and SHPB).

2.3. Conditions of dynamic compression experiments

Quasi-isentropic compression experiments were conducted on a pulsed power generator CQ-4, which can deliver pulsed currents with peak values of 3–4 MA and a rise time of 470 ns–600 ns to stripline loads.[29] A schematic of the experiment is presented in Fig. 1. Shaped electrode panels were employed to ensure the magnetic field uniformly distributed across the loading surface and the planar propagation of pressure through the thickness of the electrode panels.[30,31]

The experimental conditions of quasi-isentropic compression are shown in Table 2. The current carrying surface of the electrode panels featured a flatness of 1 μm and a surface finish of 20 nm, and it was parallel to the sample regions within a tolerance of 3 μm. In the design of the polystyrene sample dimensions, care was taken to avoid shock formation within the samples, and to prevent interference from lateral rarefaction waves and catch-up unloading waves within the testing time range. The polystyrene samples used in these experiments were diamond-turned to final dimensions of 10 mm in diameter and 0.2–0.8 mm in thickness.

To obtain the *in-situ* particle velocity from the measured velocity in the experiment, the free surface measurement and polystyrene windows were adopted (see Fig. 1). The experimental samples were coated with a 500 nm thick aluminum film at the test interface, which served to reflect the laser for velocity measurement. The velocities were measured using a dual laser heterodyne velocimetry (DLHV) system with an accuracy of better than 1%.[32] The interference signal of the up-conversion dual-source heterodyne exhibits a non-zero initial baseline frequency. During the loading stage, the frequency of the interference signal increases from the baseline as the velocity rises; specifically, the frequency of the interference signal in low-speed measurement is significantly enhanced, thereby improving the temporal resolution and measurement accuracy of the velocity.

Table 2. The experimental conditions of quasi-isentropic compression experiments. Here, a denotes the anode panel, c denotes the cathode panel, – denotes empty, and S denotes the sample.

Shot number	Electrode panel materials	Electrode panel sizes (mm)	Sample sizes (mm)	Window material
CQ4-shot-760	Al	a 26 × 12 × 1.000	S1 Φ10 × 0.298	–
			S2 Φ10 × 0.323	polystyrene
	Al	c 26 × 12 × 1.000	S3 Φ10 × 0.498	–
			S4 Φ10 × 0.496	polystyrene
CQ4-shot-764	Al	a 26 × 12 × 0.999	S5 Φ10 × 0.310	polystyrene
			S6 Φ10 × 0.489	polystyrene
	Al	c 26 × 12 × 0.999	S7 Φ10 × 0.514	polystyrene
			S8 Φ10 × 0.782	polystyrene
CQ4-shot-769	Cu	a 36 × 10 × 1.004	S9 Φ10 × 0.311	–
	Cu	a 36 × 10 × 1.004	S10 Φ10 × 0.504	–

3. Results and discussion

3.1. Compressibility and sound speed

The measured velocity histories of CQ4-shot-760, CQ4-shot-764 and CQ4-shot-769 are shown in Fig. 3. Two structures were used in the experimental design to measure the sample velocities during the loading process. One was used to measure the free surface velocity of the stepped samples, and the other was used to measure the sample/transparent window interface velocity of the stepped samples. When the wave impedance of the sample material and the window material are comparable, the reflection of the loading stress wave at the interface between the sample and the window is attenu-

ated, enabling the experimentally measured interface velocity to approximate the *in-situ* particle velocity of the samples. In this study, polystyrene was selected as the window material, which is identical to the sample material.

During the loading process, the stress wave propagating through the window material induces an additional Doppler frequency shift in the incident light wave, necessitating a correction to the measured apparent velocity. The relationship between the apparent velocity and the interface velocity can be expressed using a coefficient related to the loading pressure and the wavelength of the laser. Due to the low range of loading pressures and small temperature rise during quasi-isentropic compression, the difference in refractive indices can be neglected. Herein, the refractive index correction relationship for polystyrene windows is adopted as $u_s = 1.022u_w$,[33] where u_s denotes the interface particle velocity and u_w represents the apparent interface velocity. By applying the window refractive index correction, the *in-situ* particle velocity at the interface can be directly measured in the experiment.

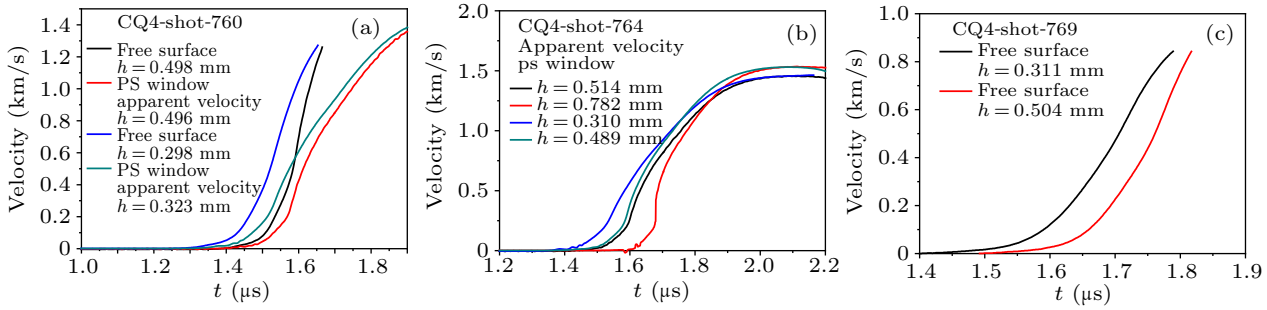


Fig. 3. The results of experimental measurement of velocity wave profiles.

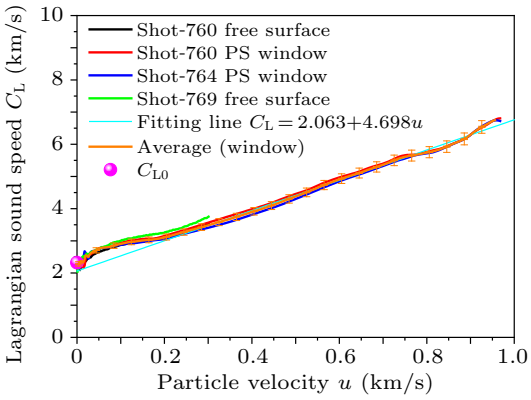


Fig. 4. The Lagrangian sound speed of polystyrene.

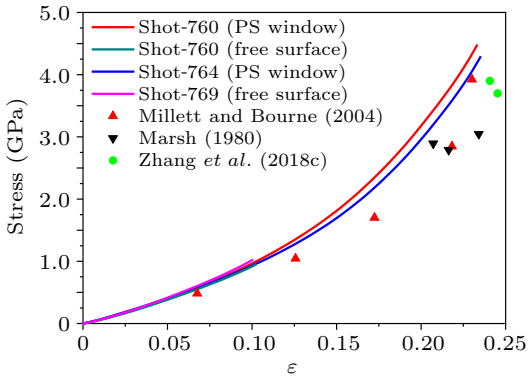


Fig. 5. Longitudinal stress obtained under ramp wave compression.

According to the data processing method mentioned above, the calculated Lagrangian sound speed of polystyrene is shown in Fig. 4. It can be seen in Fig. 4 that the Lagrangian sound speed of polystyrene exhibits a linear relationship with particle velocity, expressed as $C_L = 2.063 + 4.698u$. The results of longitudinal stress–strain under quasi-isentropic loading, calculated using Eqs. (4) and (5), are shown in Fig. 5, and the compressibility within 4 GPa under quasi-isentropic loading is experimentally obtained continuously. By comparing the quasi-isentropic compression line with the shock Hugoniot point,[11,34] it can be seen that the quasi-isentropic compression line is higher than the shock Hugoniot pressure under the same strain. With the increase in loading pressure, the difference between the quasi-isentropic compression line and Hugoniot line increases gradually.

3.2. Strength at high pressure and high strain rate

During quasi-isentropic compression, the temperature change along the quasi-isentrope is given by Refs. [25,26].

$$\mathrm{d}T = \frac{1}{c_v}\left(\frac{bT}{\rho^2}\mathrm{d}\rho + \phi\frac{2Y}{3\rho^2}\mathrm{d}\rho\right), \tag{6}$$

$$b = 3\alpha K_T, \tag{7}$$

where c_v is the specific heat at constant volume per unit mass, α is the linear coefficient of thermal expansion, $\phi = 1$ is the fraction of the plastic work converted to heat and K_T is the isothermal bulk modulus. The pressure along the quasi-isentrope is

$$\mathrm{d}P = \frac{K}{\rho}\mathrm{d}\rho + \phi\frac{2bY}{3c_v\rho^2}\mathrm{d}\rho, \tag{8}$$

where K is the isentropic bulk modulus, and $b/(c_v\rho)$ is often termed the Grüneisen parameter.

Under the fluid model assumption, the numerical calculation method for solving the isentrope using the shock Hugoniot line as the reference line of the Grüneisen equation of state

has been introduced in the literature. Under the assumption of $\gamma/\gamma_0 = V/V_0$, and a linear relationship between shock wave velocity and particle velocity, the isentrope is given by[25,26,35]

$$P_s = P_H \cdot \exp\left[-\gamma_0(\eta_H - \eta_s)\right] + \rho_0 C_0^2 \cdot \exp(\gamma_0 \eta_s) \times \int_{\eta_H}^{\eta_s} \frac{1+(\lambda-\gamma_0)\eta}{(1-\lambda\eta)^3} \cdot \exp(-\gamma_0\eta)\,\mathrm{d}\eta, \quad (9)$$

where γ is the Grüneisen parameter, V is the specific volume, $\eta = 1-\rho/\rho_0$ is the compressibility, λ and C_0 are the Hugoniot parameter in the Hugoniot relation $D = C_0 + \lambda u$, ρ_0 is the initial density, and P_H and η_H are the Hugoniot parameters of the starting point, respectively.

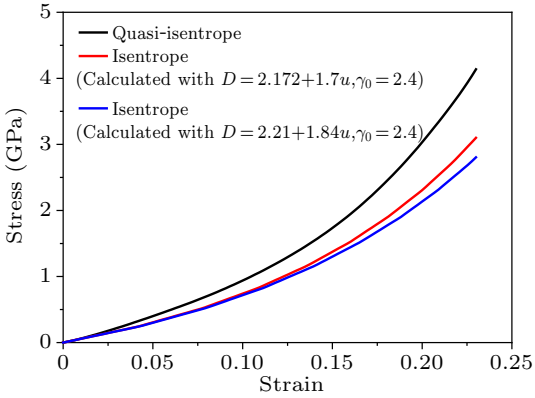


Fig. 6. The isentrope and quasi-isentrope of polystyrene.

The isentropic compression line, calculated using Eq. (9), is shown in Fig. 6. Two sets of shock Hugoniot relations are used as reference lines in the figure, namely, $D = 2.21 + 1.84u$[11,12] and $D = 2.172 + 1.7u$,[33] and the Grüneisen coefficient γ_0 is 2.4. The parameter values used in the calculation are as follows: $P_H = 0$, $\eta_H = 0$, $\nu = 0.343$, $\rho_0 = 1.05$ g/cm^3, $V_0 = 0.952$ cm^3/g and $\phi = 1$. The other parameters are intermediate variables and are not directly used in the calculation with fixed values. From the calculation results in Fig. 6, there is little difference. The second term in Eq. (8), i.e., the thermal pressure induced by plastic work, is evaluated using an approximate calculation method. Since the pressure range is small, the maximum value approximation is adopted within the pressure range of 2 GPa, and $Y = 0.4$ GPa is used. The approximate calculation of the plastic work induced by hot pressing is about 0.1 GPa, accounting for approximately 5% of the isentropic pressure. The yield strength of polystyrene can be approximately calculated from the isentropic compression line in Fig. 6 and Eq. (2). The calculated yield strength of polystyrene is shown in Fig. 7, which is obtained using the average result of the two isentropic compression lines. Using the asymptotic intersection method, the ramp elastic limit (σ_{el}) is 0.35 GPa and the calculated initial yield strength is 0.16 GPa by

$$Y_0 = \sigma_{el} \times (1-2\nu)/(1-\nu), \quad (10)$$

where Y_0 is the initial yield strength, σ_{el} is the ramp elastic limit and ν is Poisson's ratio in Table 1.

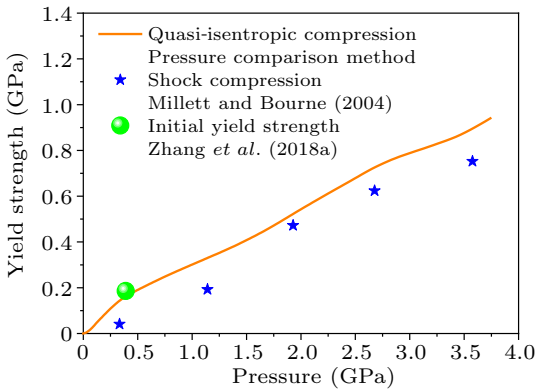


Fig. 7. The yield strength of polystyrene calculated using the elasto-plastic method.

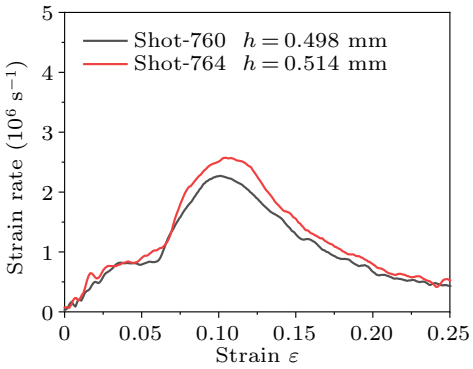


Fig. 8. The strain rates of PS quasi-isentropic experiments.

The strain rate under quasi-isentropic loading is calculated as

$$\dot{\varepsilon} = \frac{\dot{u}}{C_L(u)}. \quad (11)$$

The strain rate during experimental loading is shown in Fig. 8. During quasi-isentropic compression, all the experimental strain rates are in the vicinity of 10^6 s^{-1}. As observed in Fig. 8, a distinct inflection point exists at a strain of approximately 0.06, which corresponds to the elastic–plastic transition inflection point on the velocity curve. And the standard error of the average strain measured from experiments is approximately 0.005.[33] The pressure corresponding to this inflection point, calculated using Eq. (4), is 0.39 GPa, which is consistent with the results obtained via the asymptotic intersection method described earlier. The standard error of the elastic limit is 0.04 GPa, which is calculated based on the standard error of the strain. Using Von Mises or Tresca yield criteria under one-dimensional strain, the yield strength calculated using Eq. (10) is 0.186 GPa. The standard error of the initial yield strength is

$$\Delta Y_0 = \frac{1-2\nu}{1-\nu} \times \Delta\sigma_{el}, \quad (12)$$

where ΔY_0 is the standard error of the initial yield strength, and $\Delta\sigma_{el}$ is the standard error of the ramp elastic limit. The standard error of the initial yield strength is 0.02 GPa, which is calculated using Eq. (12).

3.3. Strain rate effect

The sharp increase in the yield strength within this range of strain rates has been termed the "up-turn phenomenon".[36] The initial yield strength versus strain rate relationships of different polymer materials are presented in Fig. 9. The strength of polymethylmethacrylate (PMMA) exhibits a very significant increase (the "up-turn" phenomenon) at strain rates ranging from 10^3 s^{-1} to10^4 s^{-1}.[37,38] However, the variation law of polystyrene is similar to that of epoxy,[39] polyvinylchloride (PVC)[40] and polycarbonate (PC),[17] with no obvious change in yield strength versus strainrate relationship. Furthermore, the Eyring model was employed to fit the experimental results of polystyrene, yielding the relationship between the yield strength and strain rate as $Y = 0.014\mathrm{e}^{0.256\log(\dot{\varepsilon})} + 0.10$. Typically, the enhanced strain rate sensitivity of the yield strength in glassy polymers is attributed to activation of particular molecular mobility, often arising from side chain motion or ring flips known as the β-transition. According to the Eyring model, the yielding of polymer material is associated with the segmental migration of its molecular domains (corresponding to the β mechanical loss peak). Nevertheless, polystyrene either lacks a β mechanical loss peak or exhibits it at an extremely low temperature, which explains why no sharp change in yield stress is observed within the existing experimental strain rate range.

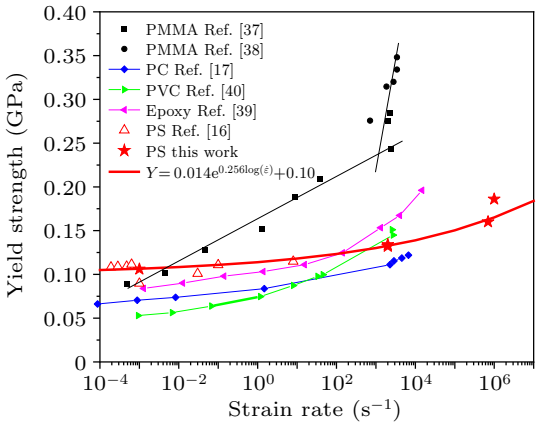


Fig. 9. The strain rate effects of the yield strength.

4. Conclusions

Experimental studies on the dynamic mechanical response of polystyrene under magnetically driven quasi-isentropic compression were conducted using a compact pulsed power generator. The velocity profiles of the samples were measured via an advanced DLHV system, and polystyrene was used as the window material to achieve impedance matching between the sample and the window, thereby enabling direct measurement of *in-situ* particle velocity. The Lagrangian analysis method was used to analyze the *in-situ* particle velocity profiles; the results indicate that the Lagrangian sound speed of polystyrene exhibits a linear relationship with particle velocity, expressed as $C_L = 2.063 + 4.698u$ under pressure up to 4 GPa. By subtracting the hydrostatic pressure from the experimentally measured longitudinal stress, the continuous variation of the yield strength of polystyrene at a strain rate of 10^6 s^{-1} was obtained within the pressure range up to 4.5 GPa. Combined with quasi-static loading and SHPB loading data, the strain rate effect of polystyrene was studied. It was found that the yield strength of polystyrene is subject to the strain rate effect; however, the underlying mechanism remains unchanged for strain rates up to 10^6 s^{-1}. Within the studied strain rate range, the Eyring model remains applicable.

Acknowledgements

This work was supported by the National Natural Science Foundation of China (Grant Nos. 12272364 and 12002327). The authors wish to thank Mr. Chao Xu, Rongjie Shui, and Gang Wu at IFP for their dedication to experimental operations on the CQ machine.

References

[1] Akbari B and Bagheri R 2016 *Mech. Mater.* **103** 11
[2] Baer M R, Hall C A, Gustavsen R L, Hooks D E and Sheffield S A 2007 *J. Appl. Phys.* **101** 034906
[3] Barrios M A, Hicks D G, Boehly T R, Fratanduono D E, Eggert J H, Celliers P M, Collins G W, Meyerhofer D D 2010 *Phys. Plasmas* **17** 056307
[4] Cauble R, Da Silva L B, Perry T S, Bach D R, Budil K S, Celliers P, Collins G W, Ng A, Jr Barbee T W, Hammel B A, Holmes N C, Kilkenny J D, Wallace R J, Chiu G and Woolsey N C 1997 *Phys. Plasmas* **4** 1857
[5] Kolsky H 1949 *Proc. Phys. Soc. Lond. Sect. B* **62** 676
[6] Davies E D H and Hunter S C 1963 *J. Mech. Phys. Solids* **11** 155
[7] Siviour C R and Jordan J L 2016 *J. Dynamic Behavior Mater.* **2** 15
[8] Walley S M, Field J E, Pope P H and Safford N A 1989 *Philos. Trans. R. Soc. Lond. A* **328** 1
[9] Walley S M, Field J E, Pope P H and Safford N A 1991 *J. Phys. III France* **12** 1889
[10] Walley S M and Field J E 1994 *Dymat. J.* **1** 211
[11] Millett J C F and Bourne N K 2004 *J. Phys. D Appl. Phys.* **37** 2901
[12] Bourne N K and Millett J C F 2008 *J. Mater. Sci.* **43** 185
[13] Zhang X P, Luo B Q, Wu G, Wang G J, Tan F L, Zhao J H and Sun C W 2018 *Mech. Mater.* **124** 1
[14] Vogler T J and Hudspeth M C 2021 *J. Dynamic Behavior Mater.* **7** 262
[15] Hudspeth M C, Olles J, Manda A, Williams J, Root S and Vogler T J 2020 *J. Appl. Phys.* **128** 205901
[16] Lee S F and Swallowe G M 2006 *J. Mater. Sci.* **41** 6280
[17] Siviour C R, Walley S M, Proud W G and Field J E 2005 *Polymer* **46** 12546
[18] Ao T 2009 *AIP Conf. Proc.* **1195** 689
[19] Remington B A, Park H S, Casey D T, Cavallo R M, Clark D S, Huntington C M, Kuranz C C, Miles A R, Nagel S R, Raman K S and Smalyuk V A 2019 *Proc. Natl. Acad. Sci. USA* **116** 18233
[20] Asay J R, Ao T, Davis J P, Hall C, Vogler T J and Gray G T 2008 *J. Appl. Phys.* **103** 083514
[21] Asay J R 2000 *AIP Conf. Proc.* **505** 261

[22] Reisman D B, Toor A, Cauble R C, Hall C A, Asay J R, Knudson M D and Furnish M D 2001 *J. Appl. Phys.* **89** 1625
[23] Davis J P, Deeney C, Knudson M D, Lemke R W, Pointon T D and Bliss D E 2005 *Phys. Plasmas* **12** 056310
[24] Fowles G R 1961 *J. Appl. Phys.* **32** 1475
[25] Vogler T J 2009 *J. Appl. Phys.* **106** 053530
[26] Vogler T J, Ao T and Asay J R 2009 *Int. J. Plast.* **25** 679
[27] Hall C A 2000 *Phys. Plasmas.* **7** 2069
[28] Ao T, Knudson M D, Asay J R and Davis J P 2009 *J. Appl. Phys.* **106** 103507
[29] Wang G J, Luo B Q, Zhang X P, Zhao J H, Sun C W, Tan F L, Chong T, Mo J J, Wu G and Tao Y H 2013 *Rev. Sci. Instrum.* **84** 015117
[30] Zhang X P, Wang G J, Zhao J H, Tan F L, Luo B Q and Sun C W 2014 *Rev. Sci. Instrum.* **85** 055110
[31] Zhang X P, Wang G J, Luo B Q, Zhang X, Wang G, Luo B, Bland S N, Tan F, Zhao F, Zhao J H, Sun C W and Liu C L 2018 *J. Alloys Compd.* **731** 569
[32] Tao T J, Weng J D and Wang X 2011 *Opto-Electron. Eng.* **38** 39
[33] Zhang X P, Wang G J, Luo B Q, Tan F L, Bland S N, Zhao J H, Sun C W and Liu C L 2018 *J. Mater. Sci.* **53** 12628
[34] Marsh S P 1980 *LASL Shock Hugoniot data* (University of California press, California) p. 296
[35] Meyers M A 1994 *Dynamic behavior of materials* (Wiley Interscience, San Diego) pp. 126–151
[36] Rosenberg Z, Kositski R, Ashuach Y, Leus V and Malka-Markovitz A 2019 *Int. J. of Solids and Struct.* **176** 185
[37] Jordan J L, Spowart J E, Kendall M J, Woodworth B and Siviour C R 2015 *Philos. Trans. R. Soc. Lond. A* **372** 20130215
[38] Rittel D and Brill A 2008 *J. Mech. Phys. Solids* **56** 1401
[39] Jordan J L, Foley J R and Siviour C R 2008 *Mech. Time-Depend Mater.* **12** 249
[40] Jordan J L, Siviour C R and Woodworth B 2012 *AIP Conf. Proc.* **1426** 191